IET Microwaves, Antennas & Propagation

Research Article

IET Journals
The Institution of Engineering and Technology

Equilateral triangular dielectric resonator based co-radiator MIMO antennas with dual-polarisation

ISSN 1751-8725
Received on 28th February 2018
Revised 14th May 2018
Accepted on 2nd July 2018
E-First on 6th September 2018
doi: 10.1049/iet-map.2018.5035
www.ietdl.org

Abhishek Sharma[1] ✉, *Anirban Sarkar*[1], *Animesh Biswas*[1], *Mohammad Jaleel Akhtar*[1]

[1]*Department of Electrical Engineering, Indian Institute of Technology Kanpur, Kanpur 208016, India*

✉ *E-mail: abhisheksharma.rf@gmail.com*

Abstract: In this study, two types of dielectric resonator antennas (DRAs) with dual-polarisation are proposed and investigated for multiple-input multiple-output (MIMO) applications. The first design is a dual-slant polarised DRA and exhibits the measured impedance bandwidth of 8.2% (5.27–5.72 GHz) and 11.2% (5.05–5.65 GHz) for *Port1* and *Port2*, respectively. Across the operating frequency band, the isolation between the input ports is better than 22 dB and the measured gain of the antenna varies in the range of 5.99–6.38 dBi. The second design developed here is a dual-linearly polarised DRA which is able to provide horizontal and vertical polarisations and is realised by integrating a two-stage rat-race coupler with the DRA for excitation purpose. In this case, the measured impedance bandwidths are 11.81% (5.18–5.83 GHz) and 15.18% (4.93–5.74 GHz) for *Port1* and *Port2*, respectively, and the inter-port isolation is better than 20 dB throughout the operating frequency band. The antenna exhibits the measured gain variation of 5.94–6.48 dBi for *Port1* and 5.54–5.86 dBi for *Port2*. Furthermore, for both the antennas, the envelope correlation coefficient is below 0.0004 throughout the bandwidth and the total active reflection coefficient is better than −10 dB, confirming the good diversity and radiation performance.

1 Introduction

With the emergence of dielectric resonator antennas (DRAs) in 1983 [1], they have gained enormous attention in the wireless communication systems because of their potential features such as light weight, small size, high radiation efficiency (due to lack of surface wave and conductor losses), relatively wide bandwidth [2]. Being a volumetric radiator (three-dimensional (3D) structure), it offers more design flexibility than the conventional planar antennas. More interestingly, the possibility of excitation of multiple orthogonal modes in a single dielectric resonator (DR) can be used to design multiple decoupled antenna ports to realise MIMO/diversity system [3, 4]. This advantage omits the need of multiple elements to realise the MIMO/diversity antenna system and makes the overall design compact.

The phenomenal growth in the wireless technology and communication demands higher data rate, strong reliability and robustness. To meet these requirements, the multiple-input multiple-output (MIMO) technology has emerged as a new paradigm and presently used in various wireless standards such as IEEE 802.11. This technology uses multiple radiators at the transmit and receive ends in order to provide superior data rate, better link reliability and spectral efficiency within the limited spectra and without any additional power requirement [5]. Over the past few years, one major aspect of DRAs research has been focused on designing MIMO/diversity antennas covering both microwave and millimetre-wave frequency band [3, 6–16].

For certain applications, dual-slant polarised antennas are preferable over the horizontal (H) and vertical (V) counterparts because of the symmetrical propagation characteristics [17]. The dual-slant polarisation adds up some advantage over H/V counterparts as demonstrated in [18] for wireless cellular communication in an urban environment and in [19] for the indoor wireless communication link. Several slant polarised and dual-slant polarised antennas have been reported [17, 20–22]. More recently, a substrate integrated waveguide fed DRA array with 45° slant polarisation has been reported and investigated in [23]. However, to the best of the author's knowledge, the dual-slant polarised antenna based on DR has not been reported earlier in the literature. It is noted that the design based on DR would result in a simple configuration along with the easy excitation mechanism.

It is mainly due to the aforementioned reasons, in this paper, a dual-slant polarised DRA is proposed and investigated. The proposed dual-slant polarised DRA is simple and compact as it uses co-radiator configuration with dual-ports instead of the separate radiator. The design uses a conformal feeding mechanism to excite the DRA in its fundamental TM_{101} mode. Next, as an extension to the dual-slant polarised antenna design, another dual-polarised DRA having vertical (V) and horizontal (H) polarisations is presented. The idea is that when the two ports of the edge fed DRA are excited simultaneously then the different linear polarisation states (i.e. vertical and horizontal) can be obtained depending on the phase of the feeding signal applied at the ports. In order to implement the feeding circuitry for simultaneous excitation, a two-stage broadband 180° hybrid coupler is utilised. The equal magnitude in-phase and out-of-phase excitation of the triangular DR by the 180° hybrid coupler generates vertical and horizontal polarised fields, respectively. Both the proposed MIMO antennas achieve high inter-port isolation and low envelope correlation. All the simulations are done in CST Microwave Studio and the prototypes are developed for experimental verification.

2 Antenna 1: dual-slant polarised DRA

Fig. 1*a* shows the geometry of the proposed 45° slant polarised DRA, where an equilateral triangular DR is placed over a grounded substrate of dimension $60 \times 60 \times 0.787\,\text{mm}^3$ and relative permittivity of 2.2. The DR under investigation is made of Rogers RT/Duroid 6010 of relative permittivity 10.2 having side length A and height H. The DR is excited in the fundamental TM_{101} mode using a conformal rectangular strip (width F_W and length F_H) situated at the edge of the DR. For the given dimensions of the DR, the theoretical resonant frequency calculated using the equations given in [24] is 5.12 GHz, which fairly agrees with the simulated value of 5.20 GHz (see Fig. 1*a*). The simulated impedance bandwidth of the slant polarised DRA is 11.23%, covering the frequency range of 4.96–5.55 GHz. Fig. 1*b* portrays the electric field distribution at 5.2 GHz. From the figure, it is confirmed that the fundamental TM_{101} mode is excited with the electric field vector tilted at an angle of 45°, which results in the linear slant polarisation. Fig. 1*c* depicts the simulated reflection coefficient of

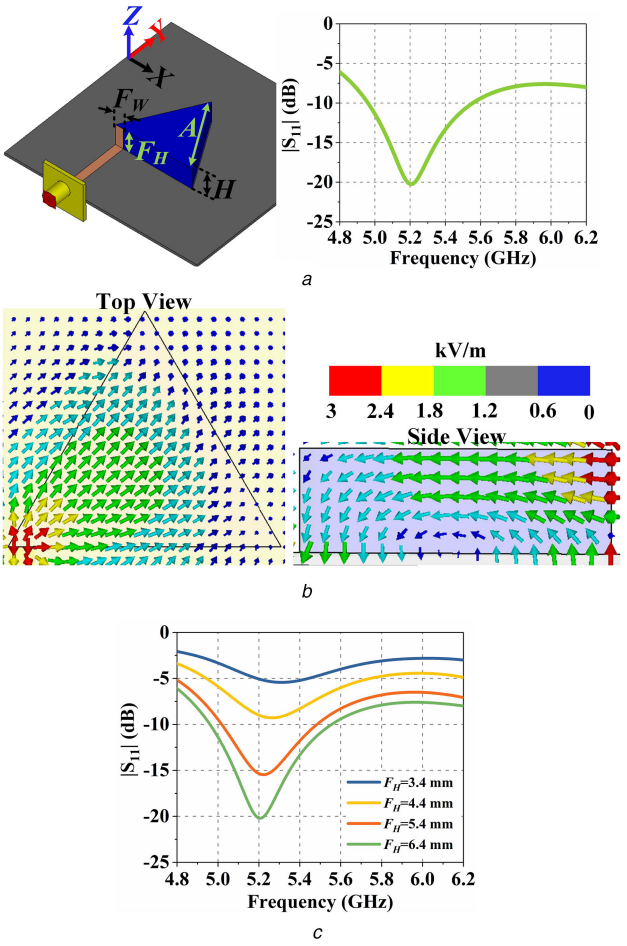

Fig. 1 *Slant polarised DRA and its simulated response*

(a) Schematic diagram of edge fed equilateral triangular DRA and its simulated response (geometrical parameters: $A = 24$, $H = 6.4$, $F_W = 2.4$, $F_H = 6.4$, (all dimensions are in mm)),

(b) Electric field distribution in DR,

(c) Simulated reflection coefficient for different values of feed length F_H

45° slant polarised DRA for different values of feed length F_H. From the figure, it can be concluded that the impedance matching gets better on increasing the value of F_H. Thus, the final value of F_H is chosen equal to the height of DRA, i.e. 6.4 mm.

Figs. 2*a* and *b* show the geometry and prototype of the proposed dual-slant polarised DRA. The proposed antenna is fed using a conformal rectangular strip and the two ports of the antenna are situated at the opposite edge of the DR. In this case, the side of the DR containing the feed is perturbed in the form of the semi-cylindrical geometry of diameter D and height H. The simulated response of the dual-slant polarised DRA for different values of D is shown in Figs. 2*c* and *d*. Due to perturbation the effective permittivity reduces and as a result of the resonant frequency shifts to the higher side without affecting the impedance matching. It is worth mentioning here that the perturbation in the DR improves the isolation between the input ports across the bandwidth. Table 1 summarises the isolation over the operating frequency band for different values of D. In conclusion, the final value of D is chosen as 10 mm for which the isolation is better than 30 dB across the frequency band (5.22–5.94 GHz), which almost covers the 5-GHz WLAN band and UNII frequency spectrum. The theoretical resonant frequency for the perturbed case can be calculated using the equations given in [24] by replacing relative permittivity with effective permittivity which can be determined as [25]

$$\epsilon_{\text{reff}} = \frac{\epsilon_{\text{r}} V_{\text{p}} + \epsilon_{\text{a}} V_{\text{a}}}{V_{\text{p}} + V_{\text{a}}} \tag{1}$$

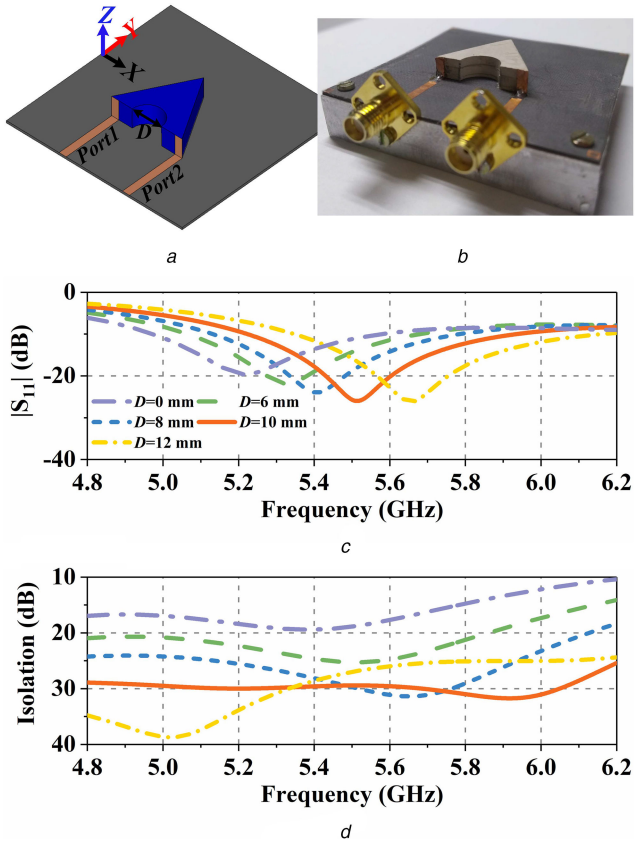

Fig. 2 *Dual-slant polarised DRA and its simulated response for different values of D*

(a) Schematic (geometrical parameter: $D = 10$ mm),

(b) Antenna prototype reflection coefficient isolation

where ϵ_{r} and ϵ_{a} are the relative permittivities of DR and perturbed region (air), respectively, V_{p} represents the volume of the perturbed DR and V_{a} is the volume of the perturbed region. Using (1) along with the equations given in [24], the theoretical resonant frequency for the case when $D = 10$ mm is 5.54 GHz which agrees with the simulated value of 5.5 GHz.

Figs. 3*a* and *b* portray the electric field distribution of dual-slant polarised DRA at 5.5 GHz and the corresponding 3D radiation patterns are shown in Figs. 3*c* and *d*. It is observed that the when the DR is excited through *Port1*, the electric field vector is tilted at an angle $\Phi = 45^{\circ}$, whereas when it is excited through *Port2* the tilt angle is $\Phi = 135^{\circ}$ and as a result dual-slant polarisation is achieved.

Fig. 4 depicts the simulated and measured responses of the proposed dual-slant polarised DRA. The simulated impedance bandwidth of the proposed antenna is 12.9% (5.22–5.94 GHz) for both the ports and the corresponding measured values are 8.2% (5.27–5.72 GHz) and 11.2% (5.05–5.65 GHz) for *Port1* and *Port2*, respectively. Over the operating bandwidth, the port-to-port isolation is better that 30 dB in simulation and 22 dB in measurement. It is noted that for the measurement purpose, the rectangular strip is made of adhesive copper tape and it is difficult to maintain a uniform contact with the DR surface and thus, it causes the deviation between the simulated and measured results. Moreover, the adhesive used to adhere the DR to the low permittivity substrate (LPS) and the air gap between the LPS and DR might affect the measurement as well. Such relative shift is not unusual in the DRA measurement which is also evident from earlier studies reported in [26, 27].

The normalised radiation pattern of the dual-slant polarised DRA at 5.5 GHz when excited through *Port1* with *Port2* terminated into the matched load is shown in Fig. 5. The proposed antenna radiates in broadside direction with the cross-polarisation level better than −15 dB along the zenith in both simulation and measurement. The simulated and measured gain of the antenna

Table 1 Antenna parameters for different values of D

Parameters	$D = 0$	$D = 6$	$D = 8$	$D = 10$	$D = 12$
f_r, GHz	5.2	5.32	5.4	5.5	5.65
BW, GHz	4.97–5.58	5.06–5.68	5.13–5.78	5.22–5.94	5.35–6.16
I, dB at f_r	18.5	23.8	28.4	29.5	25.6
IBW, dB	16.8–19.5	21.2–25.4	25–31	30–32	24–29

f_r: resonant frequency, BW: bandwidth, I: isolation, D: diameter in millimetres, IBW: isolation over bandwidth.

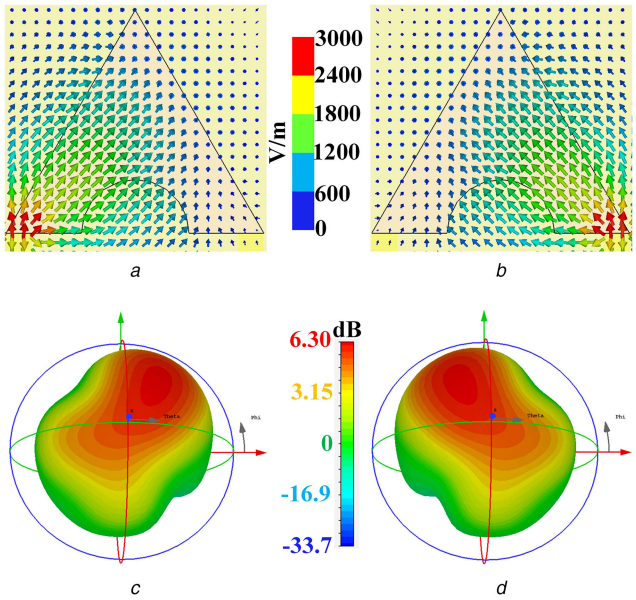

Fig. 3 *Field distribution and 3D radiation pattern*
(a) *E*-field distribution for *Port1*,
(b) *E*-field distribution for *Port2*,
(c) 3D radiation pattern for *Port1*,
(d) 3D radiation pattern for *Port2*

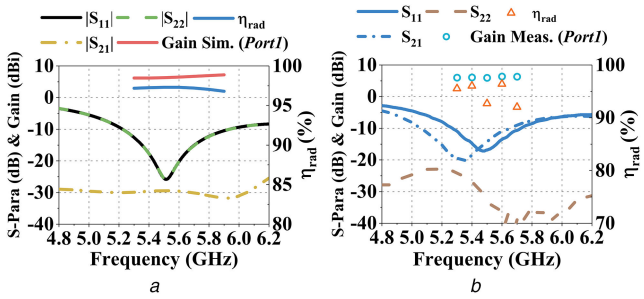

Fig. 4 *Response of the dual-slant polarised DRA*
(a) Simulated,
(b) Measured

varies in the range of 6.15–7.22 and 5.99–6.38 dBi, respectively throughout the bandwidth as depicted in Fig. 4. The simulated and measured radiation efficiencies are greater than 96 and 92%, respectively, as shown in Fig. 4.

3 Antenna 2: dual-linearly (H/V) polarised DRA

As an extension to the previous design, a dual-linearly polarised DRA having horizontal (H) and vertical (V) polarisations is designed in this section. Figs. 6*a* and *b* depict the operating principle of the H/V polarised DRA. As discussed in the previous section, when the antenna is fed separately at *Port1* (or *Port2*), it produces slant polarisation along $\Phi = 45^{\circ}$ (or $\Phi = 135^{\circ}$) direction. However, when both the ports are excited simultaneously, the vertical and horizontal polarisations are achieved depending on the phase difference ($\Delta\Psi = \Psi_1 - \Psi_2$) of the signal between the two ports. When the in-phase ($\Delta\Psi = 0^{\circ}$) equal magnitude signal is applied at the two ports, then the horizontal component of the

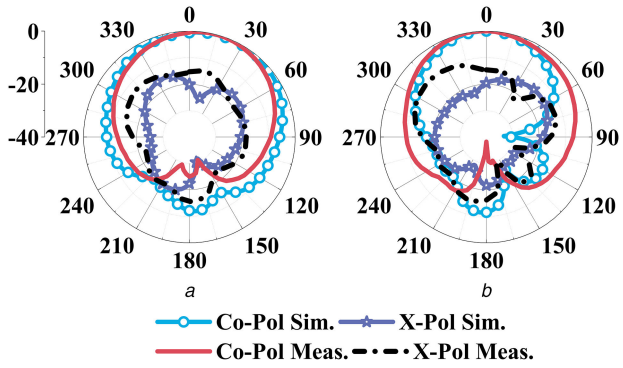

Fig. 5 *Simulated and measured normalised radiation pattern at Port1 with Port2 terminated into a matched load*
(a) $\Phi = 45^{\circ}$,
(b) $\Phi = 135^{\circ}$

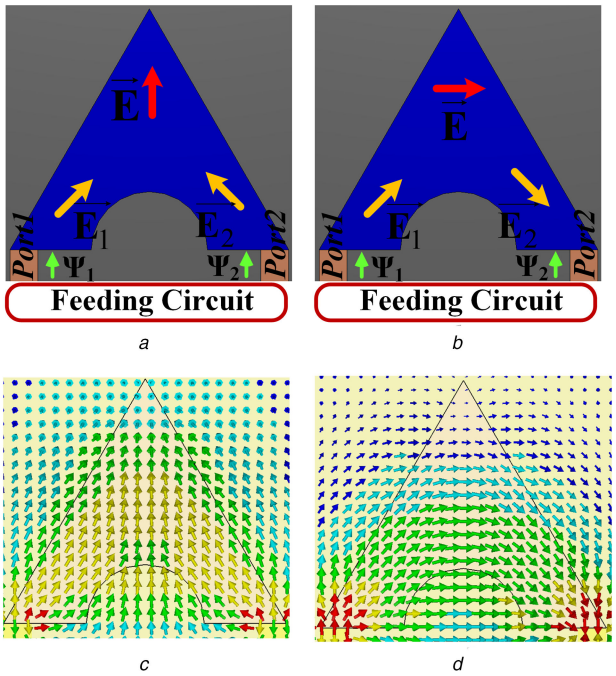

Fig. 6 *Operating principle of dual-linearly (H/V) polarised DRA*
(a) In-phase excitation,
(b) Out-of-phase excitation,
(c) *E*-field distribution with in-phase excitation,
(d) *E*-field distribution with out-of-phase excitation

electric field, i.e. E_x is cancelled out, leaving only the vertical component of the electric field, i.e. E_y as shown in Fig. 6*a*. Thus, the in-phase excitation generates vertical polarised fields. In a similar manner, when the signals at both the ports are in equal magnitude and out-of-phase ($\Delta\Psi = 180^{\circ}$), the vertical component E_y vanishes and leaving only the E_x component of the electric field (see Fig. 6*b*), thus producing horizontal polarised fields. In order to verify the above concept, the simulated electric field distributions for in-phase and out-of-phase excitation are portrayed in Figs. 6*c* and *d*, respectively. From the figure, it is observed that the electric field vectors are aligned in the direction as predicted above.

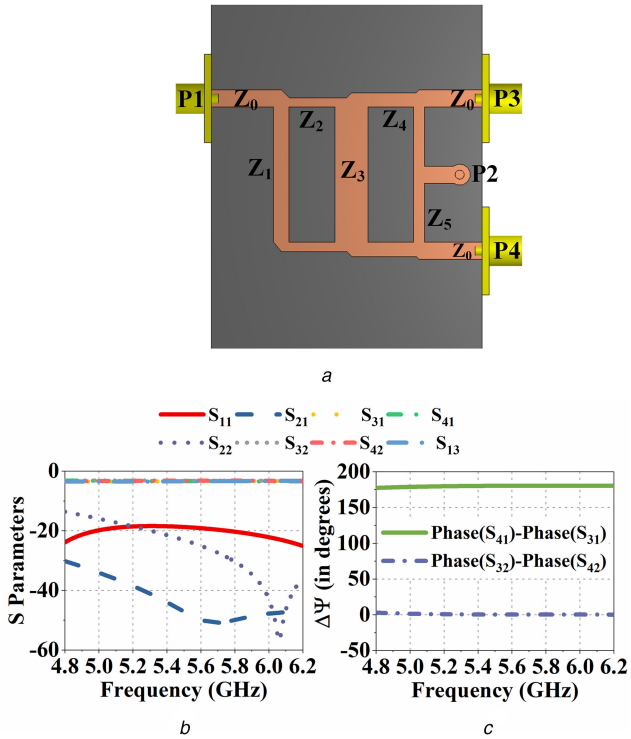

Fig. 7 *Two-stage* 180° *hybrid coupler and its response*
(a) Geometry of hybrid coupler,
(b) Simulated response

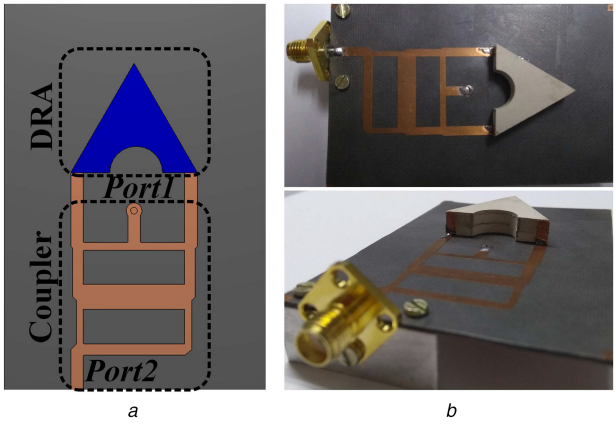

Fig. 8 *Dual-linearly (H/V) polarised DRA*
(a) Geometry of dual-linearly polarised DRA,
(b) Fabricated prototype

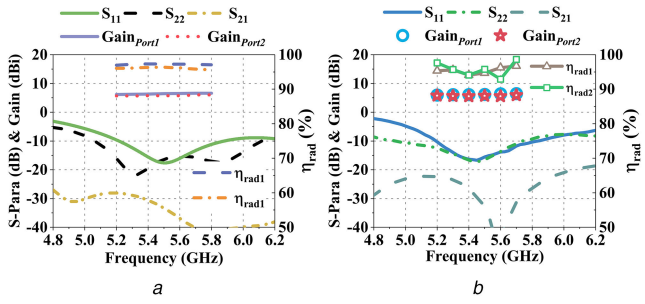

Fig. 9 *Response of the dual-linearly (H/V) polarised DRA*
(a) Simulated,
(b) Measured

The feeding circuitry for the simultaneous excitation is realised by a two-stage broadband 180° hybrid coupler as shown in Fig. 7*a*. The coupler is printed on Rogers RT/Duroid 5880 of thickness 0.787 mm and relative permittivity of 2.2. The coupler is based on the design given in [28] and it consists of three vertical $\lambda_g/2$ lines

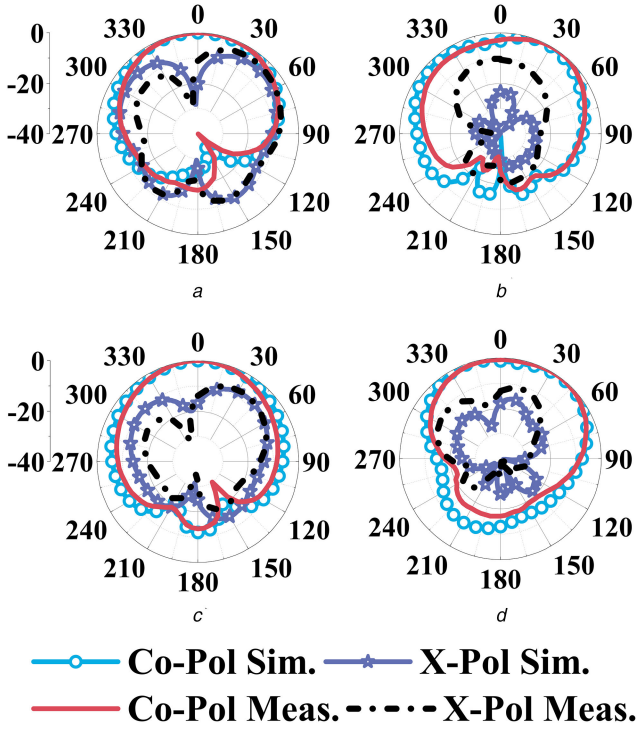

Fig. 10 *Simulated and measured normalised radiation patterns of the dual-linearly (H/V) polarised DRA at*
(a) *Port1* in *xz*-plane,
(b) *Port1* in *yz*-plane,
(c) *Port2* in *xz*-plane,
(d) *Port2* in *yz*-plane

having impedances $Z_1 = 52.9\,\Omega$, $Z_3 = 30.8\,\Omega$, $Z_5 = 66\,\Omega$ and four horizontal $\lambda_g/4$ lines having impedances $Z_2 = 74\,\Omega$ and $Z_4 = 56.5\,\Omega$. The simulated performance of the coupler is depicted in Fig. 7*b*. From the result, it can be concluded that across the working frequency band the isolation between the input ports (P1 and P2) is better than 35 dB. The phase difference between the ports P3 and P4 when fed at port P1 is 180°, whereas it is 0° when fed at port P2. The phase imbalance is under ±3°.

Fig. 8 shows the geometry and fabricated prototype of the dual-linearly polarised DRA, where the triangular DR is integrated with the 180° hybrid coupler for the excitation purpose. Here, *Port1* represents the in-phase excitation of the antenna whereas the out-of-phase excitation is given through *Port2*. The simulated and measured responses of the proposed antenna are shown in Fig. 9. For *Port1*, the simulated and measured impedance bandwidths are 12.1% (5.21–5.88 GHz) and 11.81% (5.18–5.83 GHz), respectively, whereas the corresponding values for *Port2* are 18.8% (5.06–6.11 GHz) and 15.18% (4.93–5.74 GHz), respectively. Thus, the simulated and measured overlapping impedance bandwidths are 12.1% (5.21–5.88 GHz) and 10.26% (5.18–5.74 GHz), respectively. Across the working frequency band, the isolation between the ports is >20 dB.

The normalised radiation pattern of the proposed H/V polarised DRA at 5.5 GHz for both the ports is shown in Fig. 10. It is observed that for both the ports the difference between the co-polarised and the cross-polarised field in both the planes is 10 dB along the zenith. Across the overlapping bandwidth, the simulated gain of the proposed H/V polarised DRA for *Port1* and *Port2* varies in the range of 6.14–6.58 and 5.66–6.01 dBi, respectively, and the corresponding measured values are 5.94–6.48 and 5.54–5.86 dBi, respectively, as shown in Fig. 9. The simulated radiation efficiencies for *Port1* and *Port2* are greater than 97 and 96%, respectively, and the corresponding measured values are greater than 94 and 93%, respectively.

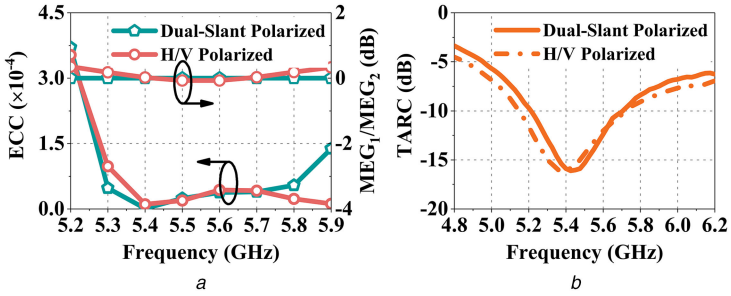

Fig. 11 *Diversity/MIMO performance*
(a) Computed envelope correlation coefficient,
(b) Measured total active reflection coefficient

Table 2 Comparison of proposed antennas with other related antennas

Reference	No. of ports	Overlapping bandwidth	Minimum isolation, dB	Gain, dBi	Antenna profile (λ_0)	Maximum ECC	Radiation efficiency, %
[3]	2	7.4% (3.78–4.07 GHz)	17	5.1–5.3[a] 1.7–2.1[b]	0.27	0.01	NA
[7]	2	7.9% (5.46–5.9 GHz)	35	NA	0.2	NA	NA
[8]	2	7% (3.6–3.86 GHz)	25	5.85–6.45[a] 4.05–6.30[b]	0.21	NA	NA
[10]	3	4.5% (2.4–2.51 GHz)	24.4	2.26[a] 2.51[b] 2.49[c]	0.27	0.001	NA
[16]	2	11.5% (4.9–5.5 GHz)	30	4.5[a] 5[b]	0.17	0.001	NA
dual-slant polarised antenna	2	7% (5.27–5.65 GHz)	22	5.99–6.38	0.13	0.0004	>92%
dual-linearly polarised antenna	2	10.26% (5.18–5.74 GHz)	22	5.94–6.48[a] 5.54–5.86[b]	0.13	0.0004	>93%

NA: not available.
[a]Gain at Port1.
[b]Gain at Port2.
[c]Gain at Port3.

4 Diversity performance

The diversity/MIMO performance of the proposed antenna is evaluated in terms of envelope correlation coefficient (ECC), mean effective gain (MEG) and total active reflection coefficient (TARC). ECC between the *i*th and *j*th antenna elements is computed using far-field pattern based formulae as suggested in [29]. Fig. 11*a* depicts the computed ECC of both dual-slant polarised and dual-linearly (H/V) polarised DRA, assuming the uniform outdoor environment. The obtained values of ECC are <0.0004 throughout the bandwidth for both the antennas which are desired for good diversity performance [5]. The MEG ratio MEG_i/MEG_j (in dB) is also computed for the desired frequency range. From the figure, it is concluded that for both the antennas the ratio remains close to 0 dB as suggested in [30].

In order to characterise the bandwidth and radiation performance of the multiport antenna, TARC is evaluated. It accounts for the mutual coupling between the elements and random-signal combinations between the ports. TARC for *N* port antenna system is defined as the ratio of square root of total reflected power to the square root of total incident power [5]

$$\Gamma_a^t = \sqrt{\frac{\sum_{i=1}^{N}|b_i|^2}{\sum_{i=1}^{N}|a_i|^2}} \tag{2}$$

where a_i is the incident signal, b_i is the reflected signal and both are related to scattering parameters as $\boldsymbol{b} = [S]\boldsymbol{a}$. For two-port MIMO system, TARC in terms of scattering parameters can be written as [31]

$$\Gamma_a^t = \frac{\sqrt{\left|\left(S_{11} + S_{21}e^{j\theta}\right)\right|^2 + \left|\left(S_{21} + S_{22}e^{j\theta}\right)\right|^2}}{\sqrt{2}} \tag{3}$$

Considering more than 30 excitation vector the measured average TARC is plotted in Fig. 11*b*. The TARC curve retains the original characteristics of the single antenna with a slight change in the operating frequency and bandwidth. This is because TARC takes into account the effects of the mutual coupling and the random phase of the incident wave.

The comparison of the proposed antenna with previously published literature is tabulated in Table 2. It is observed that the antenna has a low profile as compared to the others and achieves the better characteristics with simple design and feeding mechanism.

5 Conclusion

In this paper, two kinds of co-radiator MIMO DRAs with polarisation diversity have been proposed for wireless communication systems. The proposed antennas have been designed using an equilateral triangular DR and are excited by a conformal rectangular strip situated at the edge of the DR. The first antenna is a dual-slant polarised DRA and exhibits an impedance bandwidth of 8.2 and 11.2% for *Port1* and *Port2*, respectively. The second one is a dual-linearly polarised antenna which is able to generate vertical and horizontal polarisations depending on the phase of the feeding signal at the two ports. This exhibits the impedance bandwidths of 11.81% (5.18–5.83 GHz) for *Port1* and 15.18% (4.93–5.74 GHz) for *Port2*. Both the antennas exhibit inter-port isolation better than 20 dB throughout the bandwidth. It

has also been found that for both the diversity DRAs the envelope correlation coefficient is well below the prescribed limits and TARC is better than −10 dB, indicating the good diversity and radiation performance. The proposed antenna could be suitable for 5 GHz wireless local area (WLAN) frequency band and UNII frequency band and 5G applications.

6 References

[1] Long, S., McAllister, M., Shen, L.: 'The resonant cylindrical dielectric cavity antenna', *IEEE Trans. Antennas Propag.*, 1983, **31**, (3), pp. 406–412

[2] Petosa, A.: '*Dielectric resonator antenna handbook*' (Artech House, Boston, 2007)

[3] Zou, L., Abbott, D., Fumeaux, C.: 'Omnidirectional cylindrical dielectric resonator antenna with dual polarization', *IEEE Antennas Wirel. Propag. Lett.*, 2012, **11**, pp. 515–518

[4] Abdalrazik, A., El-Hameed, A.S.A., Abdel-Rahman, A.: 'A three-port MIMO dielectric resonator antenna using decoupled modes', *IEEE Antennas Wirel. Propag. Lett.*, 2017, **16**, pp. 3104–3107

[5] Sharawi, M.S.: '*Printed MIMO antenna engineering*' (Artech House, Boston, 2014)

[6] Guo, Y.X., Luk, K.M.: 'Dual-polarized dielectric resonator antennas', *IEEE Trans. Antennas Propag.*, 2003, **51**, (5), pp. 1120–1124

[7] Tang, X.R., Zhong, S.S., Kuang, L.B., *et al.*: 'Dual-polarised dielectric resonator antenna with high isolation and low cross-polarisation', *Electron. Lett.*, 2009, **45**, (14), pp. 719–720

[8] Gao, Y., Feng, Z., Zhang, L.: 'Compact CPW-fed dielectric resonator antenna with dual polarization', *IEEE Antennas Wirel. Propag. Lett.*, 2011, **10**, pp. 544–547

[9] Yan, J.B., Bernhard, J.T.: 'Design of a MIMO dielectric resonator antenna for LTE femtocell base stations', *IEEE Trans. Antennas Propag.*, 2012, **60**, (2), pp. 438–444

[10] Fang, X.S., Leung, K.W., Luk, K.M.: 'Theory and experiment of three-port polarization-diversity cylindrical dielectric resonator antenna', *IEEE Trans. Antennas Propag.*, 2014, **62**, (10), pp. 4945–4951

[11] Roslan, S.F., Kamarudin, M.R., Khalily, M., *et al.*: 'An MIMO rectangular dielectric resonator antenna for 4G applications', *IEEE Antennas Wirel. Propag. Lett.*, 2014, **13**, pp. 321–324

[12] Sharma, A., Sarkar, A., Biswas, A., *et al.*: 'A polarization diversity substrate integrated waveguide fed rectangular dielectric resonator antenna'. 2016 Asia-Pacific Microwave Conf. (APMC), 2016, pp. 1–4

[13] Sharma, A., Biswas, A.: 'Wideband multiple-input multiple-output dielectric resonator antenna', *IET Microw. Antennas Propag.*, 2017, **11**, (4), pp. 496–502

[14] Sharma, A., Sarkar, A., Biswas, A., *et al.*: 'Dual-band multiple-input multiple-output antenna based on half split cylindrical dielectric resonator', *J. Electromagn. Waves Appl.*, 2018, **32**, (9), pp. 1152–1163

[15] Sharawi, M.S., Podilchak, S.K., Hussain, M.T., *et al.*: 'Dielectric resonator based MIMO antenna system enabling millimeter-wave mobile devices', *IET Microw. Antennas Propag.*, 2017, **11**, (2), pp. 287–293

[16] Das, G., Sharma, A., Gangwar, R.K.: 'Dual feed MIMO cylindrical dielectric resonator antenna with high isolation', *Microw. Opt. Technol. Lett.*, 2017, **59**, pp. 1686–1692

[17] Pan, Y.M., Zheng, S.Y., Hu, B.J.: 'Singly-fed wideband 45° slant-polarized omnidirectional antennas', *IEEE Antennas Wirel. Propag. Lett.*, 2014, **13**, pp. 1445–1448

[18] Nishimori, K., Makise, Y., Ida, M., *et al.*: 'Channel capacity measurement of 8×2 MIMO transmission by antenna configurations in an actual cellular environment', *IEEE Trans. Antennas Propag.*, 2006, **54**, (11), pp. 3285–3291

[19] Vallozzi, L.: 'Patch antenna with slanted ±45° dual polarization and performance comparison with H/V diversity'. 2016 10th European Conf. on Antennas and Propagation (EuCAP), 2016, pp. 1–5

[20] Quan, X., Li, R., Fan, Y., *et al.*: 'Analysis and design of a 45° slant polarized omnidirectional antenna', *IEEE Trans. Antennas Propag.*, 2014, **62**, (1), pp. 86–93

[21] Zheng, D.Z., Chu, Q.X.: 'A multimode wideband ±45° dual-polarized antenna with embedded loops', *IEEE Antennas Wirel. Propag. Lett.*, 2017, **16**, pp. 633–636

[22] Komandla, M.V., Mishra, G., Sharma, S.K.: 'Investigations on dual slant polarized cavity-backed massive MIMO antenna panel with beamforming', *IEEE Trans. Antennas Propag.*, 2017, **65**, (12), pp. 6794–6799

[23] Abdallah, M., Wang, Y., Abdel-Wahab, W.M., *et al.*: 'Design and optimization of SIW center-fed series rectangular dielectric resonator antenna array with 45° linear polarization', *IEEE Trans. Antennas Propag*, 2017, **65**, (12), pp. 6794–6799

[24] Maity, S., Gupta, B.: 'Theoretical investigations on equilateral triangular dielectric resonator antenna', *IET Microw. Antennas Propag.*, 2017, **11**, (2), pp. 182–192

[25] He, Y., Lin, Y., Deng, C., *et al.*: 'Annular column loaded cylindrical dielectric resonator antenna for wideband conical radiation', *IEEE Trans. Antennas Propag.*, 2015, **63**, (12), pp. 5874–5878

[26] Chu, L.C.Y., Guha, D., Antar, Y.M.M.: 'Conformal strip-fed shaped cylindrical dielectric resonator: improved design of a wideband wireless antenna', *IEEE Antennas Wirel. Propag. Lett.*, 2009, **8**, pp. 482–485

[27] Guha, D., Antar, Y.M.M.: 'New half-hemispherical dielectric resonator antenna for broadband monopole-type radiation', *IEEE Trans. Antennas Propag.*, 2006, **54**, (12), pp. 3621–3628

[28] Caillet, M., Clenet, M., Sharaiha, A., *et al.*: 'A compact wide-band ratrace hybrid using microstrip lines', *IEEE Microw. Wirel. Compon. Lett.*, 2009, **19**, (4), pp. 191–193

[29] Sharawi, M.S.: 'Current misuses and future prospects for printed multiple-input, multiple-output antenna systems [wireless corner]', *IEEE Antennas Propag. Mag.*, 2017, **59**, (2), pp. 162–170

[30] Karaboikis, M.P., Papamichael, V.C., Tsachtsiris, G.F., *et al.*: 'Integrating compact printed antennas onto small diversity/MIMO terminals', *IEEE Trans. Antennas Propag.*, 2008, **56**, (7), pp. 2067–2078

[31] Chae, S.H., Keun Oh, S., Park, S.O.: 'Analysis of mutual coupling, correlations, and TARC in wibro MIMO array antenna', *IEEE Antennas Wirel. Propag. Lett.*, 2007, **6**, pp. 122–125